Properties and dynamics of the image potential states on graphite investigated by multiphoton photoemission spectroscopy

J. Lehmann, M. Merschdorf, A. Thon, S. Voll, and W. Pfeiffer*
Physikalisches Institut, Universität Würzburg, D-97074 Würzburg, Germany
(Received 1 June 1999)

Multiphoton photoemission spectroscopy of graphite using 267 nm (4.65 eV) and 400 nm (3.1 eV) excitation wavelength reveals spectroscopic features that allow the identification of the multiphoton excitation process and that correspond to the known bulk band structure. In addition, the $n=1$ and $n=2$ image potential states on graphite are identified, with binding energies of 0.85 and 0.15 eV, respectively. They are characterized by a vanishing quantum defect and are located close to the top of the band gap in the projected bulk band structure. Accordingly, the $n=1$ image potential state and the minimum of the interlayer band are both located about 4 eV above the Fermi level. This settles the ambiguities in the interpretation of the unoccupied band structure of graphite with respect to the energetic location of the interlayer band. Time-resolved two-photon photoemission spectroscopy yields a lifetime of 40 ± 6 fs for the $n=1$ image potential state. This rather long lifetime of an image potential state at the top of the band gap and the vanishing quantum defect are attributed to the two-dimensional structure of graphite. [S0163-1829(99)09547-8]

I. INTRODUCTION

Image potential states on surfaces have received considerable attention during the last years. This is mostly due to the fact that the formation of bound image potential states is a quite common phenomenon on a large variety of different surfaces and they can therefore be used to investigate and compare the electronic properties of different surfaces. In addition, the recent developments in ultrafast laser spectroscopy allow direct time-resolved investigation of the dynamics of the image potential states.[1–6] The attractive Coulomb interaction between an electron located in front of the surface and its image charge and a repulsive barrier towards the bulk arising from a gap in the projected bulk band structure leads to the formation of bound image potential states. Although their existence was proposed previously in 1939 by Shockley,[7] they were derived from detailed theoretical considerations by Echenique and Pendry[8] using multiple-reflection theory[9] and later verified and investigated by inverse photoemission spectroscopy[10–13] and two-photon photoemission spectroscopy (2P-PES).[1–6,14–16] Due to the collective character of the excitation, i.e., the polarization of bulk electrons, the formation of image potential states does not depend on the exact structural properties of the surface and is therefore a quite universal phenomenon. It is important to note, however, that their actual properties like binding energy and lifetime are determined by the bulk properties of the material.

Whereas the properties of the image potential states are known for a large number of metal surfaces,[4,13] there is very limited information available for semimetals and layered materials. To our knowledge the existence of image potential states on semimetals was only demonstrated for Sb and TiS_2.[13] For graphite an image potential state has been proposed,[13] but an unambiguous experimental evidence has been missing up to now. This is due to ambiguities in the interpretation of experiments performed to determine the unoccupied band structure of graphite. Whereas the occupied bulk band structure of graphite is well understood and different theoretical and experimental observations converge, this is not the case for the bound unoccupied states.[17] The experimental investigation of the unoccupied states of graphite started with the work of Fauster *et al.* in the early 1980s using angular-resolved inverse photoemission spectroscopy (ARIPES).[18] The authors report two unoccupied bands at about 4 eV above the Fermi energy, one of which shows dispersion along the *c* axis and the other does not. Both were attributed to the lowest unoccupied σ band that exhibits high electron densities between the carbon planes and is therefore denoted as interlayer band. The band with vanishing dispersion perpendicular to the surface was identified either as a surface state split-off from the bottom of the interlayer band or as a spectroscopic feature due to a nondirect transition to the interlayer band itself.[18] The latter observation is supported by the observation that surface modifications like the exposure to reactive oxygen and hydrogen[19] do not influence the inverse photoemission signal at 3.6 eV above the Fermi energy. However, discrepancies between these observations and the results from angular-resolved secondary electron emission spectroscopy[20,21] as well as from target current spectroscopy[22,23] initiated a controversy concerning this interpretation. Summarizing, the experimental evidence allows the placement of the minimum of the interlayer band either at about 4 or at 7.5 eV above the Fermi energy. To complicate the situation even more, both interpretations are supported by theoretical calculations, by Holzwarth *et al.*[24] for the lower interlayer band minimum and by Tatar and Rabii[25] for the placement at 7.5 eV.

Tentative interpretations of the feature at about 4 eV above the Fermi energy in terms of an image potential state are given, based on the quenching of the state by an accidental surface contamination[22] or derived from an inconsistency between experiment and theory.[26] However, it remained impossible to distinguish between an image potential state, an intrinsic surface state or effects due to the bottom of the

interlayer band. As a technique that gives information about the unoccupied band structure, two-photon photoemission spectroscopy[14,15] (2P-PES) and its time-resolved counterpart[1,27,28] is well suited to identify the nature of the electronic state seen at about 4 eV above the Fermi energy.

The dynamic properties of an excitation are either reflected by its homogeneous linewidth or can be directly investigated by time-resolved methods. Since image potential states reside in front of the surface and have a small overlap with the bulk electronic states their lifetime is in the range of 10–100 fs.[8] Usually this gives rise to a rather narrow linewidth of the photoemission peaks and allows us to apply time-resolved 2P-PES, as has been demonstrated by Schoenlein *et al.*[1] for the $n=1$ image potential state on Ag(100). In contrast to linewidth measurements that are limited by inhomogeneous line-broadening effects,[4,15] time-resolved methods can identify different contributions to the dynamic behavior of an excitation.[2,3,5,29,30]

Recent experiments have demonstrated that the hot electron relaxation in graphite deviates from the Fermi-liquid behavior of a three-dimensional electron gas.[6,31] Since both the image potential states and the bulk electronic structure exhibit two-dimensional character, one can expect a close relation between them, i.e., the lifetime of the image potential states should also deviate from the behavior of the corresponding excitation in a three-dimensional system.

In this paper we present results of multiphoton photoemission spectroscopy and time-resolved 2P-PES measurements of highly oriented pyrolytic graphite (HOPG). In the following we give a short survey of the experiment. The analysis of the single-photon and multiphoton photoemission spectra obtained after 400 nm (3.1 eV) and 267 nm (4.65 eV) excitation of the pure HOPG surface allows us to identify all observed spectral features, especially the $n=1$ and $n=2$ image potential states on graphite. Time-resolved 2P-PES for the $n=1$ image potential state is then presented and discussed in terms of optical Bloch equations for a two-level system. Finally, we discuss the close relation between the properties of the image potential states and the layered structure of graphite.

II. EXPERIMENTAL DETAILS

A. Sample preparation

The samples used for the experiments consist of highly oriented pyrolytic graphite (HOPG).[32] In contrast to single crystals of graphite, HOPG is a polycrystalline material with uniform *c*-axis orientation of the crystallites but random orientation of their basal planes that is available in high purity. The surface quality of an artificial graphite single crystal turned out to be insufficient for our experiments. The samples are cleaved either *in situ* under UHV conditions (1×10^{-10} mbar) or under ambient conditions immediately before transfer into the UHV load-lock chamber. In the latter case the samples are heated (60 min, 600 °C) to allow for stable tunneling conditions in an *in situ* UHV-STM. After this treatment the scanning tunneling microscopy (STM) topography shows no significant traces of surface contamination and we observe no differences in the photoemission spectra from *ex situ* and *in situ* cleaved samples. The quality of the cleaved HOPG surfaces is routinely characterized by *in situ* STM.

B. Time-of-flight spectrometer

The photoemission spectra are measured with a home-built UHV time-of-flight (TOF) spectrometer. The arrival times of the individual electrons are detected by a fast multichannel plate detector (MCP) in combination with a time-to-amplitude converter (TAC). Laser intensities are usually attenuated so that the probability to detect one photoelectron per laser pulse is below 0.1 and saturation of the TAC as well as space charge effects are avoided. In order to reduce the influence of stray fields between sample and spectrometer an extraction bias of 5 V is applied.

The time-of-flight of an electron is determined by the electrostatic potential between sample and MCP detector and its initial kinetic energy. Therefore, the work function difference ΔW between sample and spectrometer influences the time-of-flight of an electron. To correct for this influence we routinely determine ΔW. To achieve this the electrostatic potential between sample and detector is determined by solving the Poisson equation under the given boundary conditions.[33] The proper ΔW is found by comparing the calculated time-of-flight with the measured one. Using ΔW a relation between the time-of-flight and the kinetic energy of the emitted electrons is obtained. This relation is used for the coordinate transformation that is necessary to obtain the photoemission spectrum as a function of the kinetic energy of the electrons with respect to the sample surface.

The energy resolution of the spectrometer can be estimated from the shape of the photoemission spectrum of a material with high density of states at the Fermi energy. From the spectral shape that corresponds to the emission from states close to the Fermi energy we estimate an energy resolution of about 60 meV at a kinetic energy of 1.5 eV. Due to the shorter time-of-flight this resolution decreases for electrons with higher kinetic energy. From the calculated trajectories we estimate an angular acceptance of the spectrometer of about $\pm10°$ for electrons with 2 eV kinetic energy.

C. Two-photon photoemission spectroscopy

In our experiments we employ a home-built Ti:sapphire laser system. The stretched output of the femtosecond oscillator (80 MHz, 4 nJ, 45 fs, 800 nm) seeds a high repetition rate regenerative amplifier. The amplified laser pulses are compressed and pulses of 65 fs duration and 2–3 μJ energy are obtained at a repetition rate of up to 300 kHz. In Fig. 1 the experimental setup is shown schematically. Second-harmonic generation and sum frequency generation in two 100 μm thick BBO crystals are used to obtain laser pulses at 400 and 267 nm. The energy per pulse at both wavelengths is 20–30 nJ. A Mach-Zehnder interferometer generates pump and probe pulses with variable time delay. Two prism compressors compensate the material induced increase of pulse duration. A fused silica lens with 200 mm focal length is used to focus the laser beam on the sample.

Time-resolved 2P-PES requires the energy resolved recording of pump-probe spectra. Since the detection of electrons from the whole energy spectrum with every laser pulse

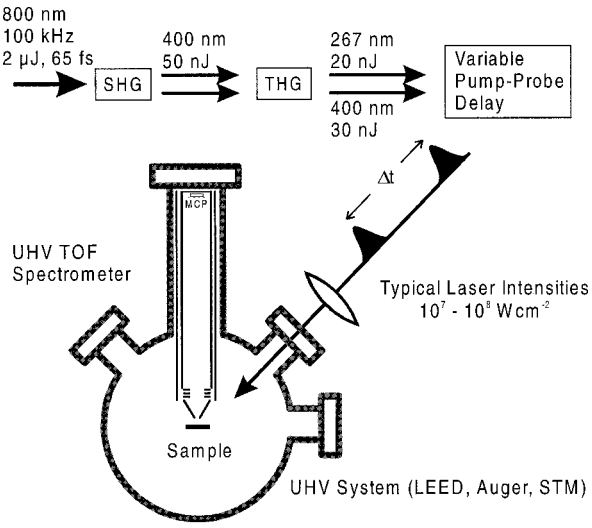

FIG. 1. Schematic representation of the experimental setup.

is one of the major advantages of the TOF technique, it is also desirable to measure the total spectrum for a given delay time and then move on to the next. To allow this kind of measurement we have tuned the laser system to high long-term stability. The typical drift of the on-line monitored pulse duration of the amplified laser pulses is less than 5 fs in 24 h. In order to check for artifacts due to laser drift or due to deterioration of the sample surface we record the photoelectron signal in repeated scans of the pump-probe delay.

III. RESULTS

A. Multiphoton photoemission from graphite

1. Photoemission at 267 nm excitation

Photoemission spectra obtained at excitation with 267 nm light (4.65 eV) are shown in Fig. 2 for different laser intensities. The observed change of the photoemission spectra with increasing laser intensity shows that the spectrum consists of at least two contributions. At the lowest excitation intensity (dotted line) a narrow peak with an exponential decrease extending to about 0.4 eV kinetic electron energy is

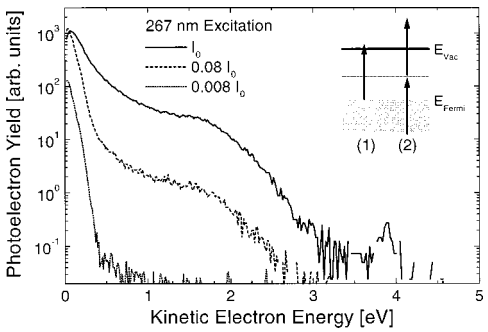

FIG. 2. Photoemission spectra of HOPG after excitation with 267 nm (4.65 eV) at different laser intensities (I_0 is 10^8 W cm^{-2}). The energy scale reflects the initial kinetic energy of the photoelectrons. The inset indicates the single-photon photoemission (1) and two-photon photoemission via the π bands at the L and M point in the Brillouin zone (2).

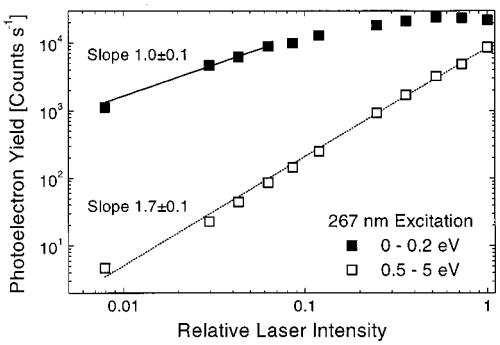

FIG. 3. Intensity dependence of the photoemission yield at 267 nm excitation integrated over final state energies between 0–0.2 eV (closed squares) and 0.5–5 eV (open squares). The continuous curves represent the fit of a power law to the data. The maximum laser intensity is 10^8 W cm^{-2}.

observed. At a ten times higher laser fluence (dashed line) the yield between 0 and 0.4 eV also increases by a factor of 10, indicating a single-photon photoemission process. However, a contribution of photoelectrons with electron energies above 0.4 eV appears and rises rapidly with increasing laser intensity.

Figure 3 displays the integrated photoelectron yield at kinetic electron energies below 0.2 eV and between 0.5 and 5.0 eV as a function of the laser intensity. At low laser intensities the yield below 0.2 eV exhibits a linear slope. The saturation of the photoemission yield at high laser intensity is attributed to the saturation of the time-to-amplitude converter. The linear relation together with the observation that the photoemission yield in this energy range neither depends on the size of the laser focus nor on the actual laser pulse duration proves that these photoelectrons stem from a single-photon photoemission process. In contrast, the photoelectron yield integrated between 0.5 and 5.0 eV shows a constant slope of 1.7 ± 0.1 over two orders of magnitude in laser intensity. We, therefore, attribute it to a two-photon photoemission process.

In order to assign the energetic position of an intermediate state with respect to the Fermi energy it is necessary to determine the work function. The presence of single-photon photoemission at 267 nm indicates that the work function of the HOPG surface must be smaller than the photon energy of 4.65 eV. In a semimetal the density of states at the Fermi energy is small or vanishes completely. The identification of the final-state energy of the photoelectrons stemming from initial states at the Fermi energy therefore requires an extrapolation of the spectrum. We estimate a work function of 4.5 ± 0.1 eV from linear extrapolation of one-photon photoemission spectra obtained at low laser intensity. This method is reasonable since the occupied and unoccupied π bands exhibit linear dispersion at the Fermi energy. The obtained value of 4.5 eV for the work function is considerably smaller than the literature value of 4.7 eV for the pure graphite surface.[23] However, since neither cleaning of the surface by either sputtering or heating nor *in situ* cleavage of the HOPG did change its work function, we believe that the observed reduction is not due to adsorbates but is an intrinsic property of the used HOPG material.

The two-photon contribution extends to about 4.5 eV kinetic electron energy. The dominant feature in the spectrum is a broad shoulder at about 2 eV final-state energy. It is

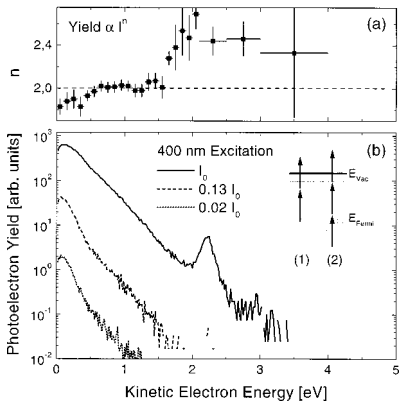

FIG. 4. The lower part (b) shows three photoemission spectra from HOPG after 400 nm excitation at different laser intensities (I_0 is 10^9 W cm^{-2}). The inset represents the nonresonant two-photon photoemission (1) and the resonant three-photon photoemission process via the $n=1$ image potential state (2). In the upper part (a) the exponent n of the power law describing the intensity dependence of the photoemission yield is displayed as a function of the kinetic electron energy. The data used for the fit stem from a sequence of ten photoemission spectra recorded in the intensity range of 10^7-10^9 W cm^{-2}.

related to a feature seen in angular-resolved inverse photoemission spectroscopy (ARIPES) at an energy of about 1.5–2 eV above the Fermi energy.[22] This feature was attributed to non-$k_\parallel$-conserving transitions from the initial state into a high density of unoccupied states of the π bands at the M and L point in the Brillouin zone. It is interesting to note that the transition energies between occupied and unoccupied π bands at the M and L point are between 4.5 and 4.7 eV,[22,17,34] and therefore very close to our excitation wavelength. Accordingly, we attribute the shoulder in the two-photon photoemission spectrum to a resonant two-photon excitation at the M and L point. At final states above 2 eV final-state energy this mechanism vanishes, since these states can no longer be reached via the unoccupied π bands at the M and L point. The alternative explanation of the shoulder due to direct two-photon photoemission from the high density of states at the σ-band maximum[6] can be ruled out, since angular-resolved photoemission reveals the σ-band maximum at 4–5 eV below the Fermi energy.[35,36]

At kinetic electron energies above 2 eV the photoemission yield declines rapidly and only a small photoemission yield is observed above 3 eV. This reflects a decrease of the density of states in the initial, the intermediate or the final state. In order to obtain spectroscopic information of the small peak at 3.9 eV kinetic electron energy long spectrum integration times are required. The origin for this emission peak is the presence of an image potential state at the surface of HOPG and will be more thoroughly discussed in Sec. III B.

2. Photoemission at 400 nm excitation

Photoemission spectra using an excitation wavelength of 400 nm (3.1 eV) are shown in Fig. 4(b) for different laser intensities. The highest photoelectron yield for all applied laser intensities is observed at low electron energy followed by an almost exponential decrease with increasing kinetic electron energy. Whereas the spectra recorded at the lowest and the next higher laser intensity consist only of a monotonously decreasing slope, a pronounced photoemission peak at about 2.25 eV kinetic electron energy appears in the spectrum recorded at the highest laser intensity.

The three spectra shown in Fig. 4 are chosen from a sequence of ten spectra recorded at different laser intensities. In order to evaluate the intensity dependence, the photoelectron yield at a given final-state energy as a function of the applied laser intensity is fitted with a power law. The obtained values for the exponent n are shown in the upper part of Fig. 4. Between 0.5 and 1.6 eV the photoemission yield scales quadratically with the laser intensity. This behavior and the measured work function of 4.5 eV (compare Sec. III A 1) proves that a two-photon photoemission process is responsible for the photoemission up to final-state energies of 1.6 eV. At higher energy the power law for the intensity dependence changes, indicating that three-photon photoemission starts to dominate.

Below 0.5 eV a slight decrease of the exponent is observed. Interestingly the change of the intensity dependence around 0.5 eV coincides with a small change of the slope in the photoemission spectra [Fig. 4(b)]. At the initial state 1.2 eV below the Fermi energy no distinct feature in the density of states is known neither from conventional photoemission spectroscopy nor from theoretical calculations.[17,24,25] On the other hand, the intermediate-state energy at about 1.9 eV above the Fermi energy coincides with the high density of unoccupied states of the π bands at the M and L point in the Brillouin zone.[17,19] The changing slope in the photoemission spectra as well as the reduced exponent n below 0.5 eV might, therefore, be explained by the predominant population of π-band states close to the M and L point and subsequent photoemission from these states. For the two-photon photoemission process with a final-state energy above 0.5 eV the lack of such a high density of unoccupied intermediate states leads to the quadratic power law.

As mentioned, the photoelectrons emitted with more than 1.6 eV kinetic energy originate from a three-photon photoemission process. This spectral contribution is dominated by a distinct peak at 2.25 eV final-state energy that corresponds either to resonant intermediate states 0.85 and 3.95 eV below the vacuum level or to a high density of initial states about 2.6 eV below the Fermi level. The latter two possibilities can be ruled out since both states should have been visible in the two-photon photoemission spectrum at 267 nm excitation at 2.2 and 0.7 eV final-state energy. Accordingly, there is evidence for a resonant intermediate state 0.85 eV below the vacuum level in the three-photon photoemission spectrum at 400 nm as well as in the two-photon photoemission spectrum at 267 nm. The nature of this intermediate state will be addressed more thoroughly in the following section.

B. Identification of the $n=1$ and $n=2$ image potential states

As outlined above, both the multiphoton photoemission spectra at 267 and at 400 nm excitation exhibit evidence for the presence of a resonant intermediate state close to the vacuum energy. Figure 5 shows photoelectron spectra recorded at 267 and 400 nm excitation. As discussed in Sec. III A 2 the peak at 2.25 eV in the photoemission spectrum at 400 nm excitation must be due to a resonant intermediate state in a three-photon photoemission process. At 267 nm

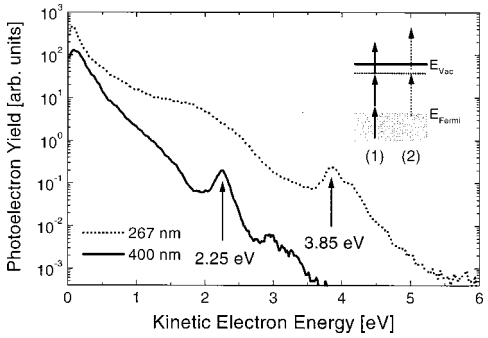

FIG. 5. Photoemission spectra of HOPG after excitation with 400 nm (solid line) and 267 nm (dotted line) light. The resonant multiphoton excitation via the $n=1$ image potential state is indicated in the inset for (1) 400 nm and (2) 267 nm excitation.

excitation a photoemission peak appears at 3.85 eV final-state energy. The difference between the final-state energy at 400 and 267 nm excitation is 1.6 eV. Within the experimental uncertainties this is in excellent agreement with the energy difference of the 400 and 267 nm photons, i.e., 1.55 eV. We therefore conclude that both photoemission peaks at 2.25 and 3.85 eV are related to the same intermediate state with a binding energy between 0.80 and 0.85 eV. Using the work function of 4.5 eV (Sec. III A 1) this corresponds to a state about 3.7 eV above the Fermi level. Whereas with 400 nm excitation, this state must be populated by a two-photon process and a third photon is required for the photoemission, it can be directly populated by the absorption of one 267 nm photon.

Experiments performed with different HOPG samples have shown that the magnitude of the photoemission peaks relative to the nonresonant background photoemission varies significantly with the quality of the cleaved surface. In addition, an exposure of the cleaved surface to the background pressure in the UHV system over several days leads to a reduction of the peak amplitudes. This indicates that the intermediate state 3.65 eV above the Fermi energy must be a surface state. However, this experimental evidence is not yet sufficient to distinguish between an intrinsic surface state and an image potential state.

Figure 6 displays a photoemission spectrum at 400 nm

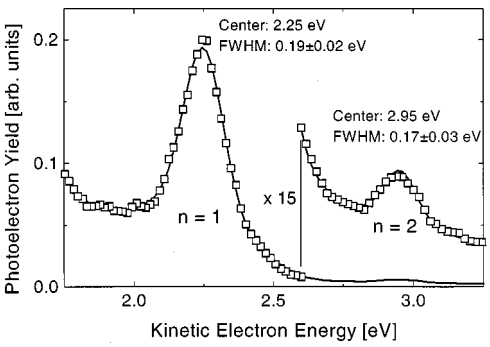

FIG. 6. Photoemission spectrum of the $n=1$ and $n=2$ image potential state at 400 nm excitation. The spectrum around the $n=2$ is multiplied by a factor of 15. The solid line corresponds to a Lorentzian fit including an exponential decrease of the background. The center and the linewidth from the fit are given for the photoemission peaks.

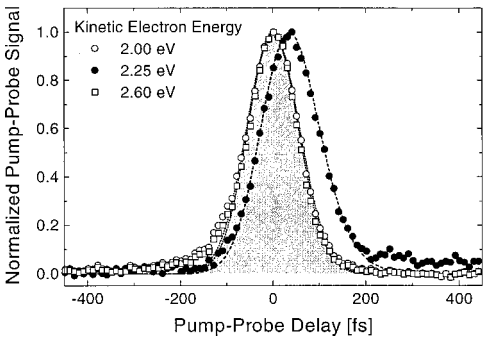

FIG. 7. Normalized pump-probe spectra for two-photon photoemission via the $n=1$ image potential state (closed symbols) and via intermediate states 0.25 eV below and 0.35 eV above this state (open symbols) are shown. The shaded area is the fit of a Gaussian to the cross correlation of pump and probe pulses as it was obtained from time resolved 2P-PES on a polycrystalline tantalum surface. The optical Bloch equations for a two-level system were used to fit the experimental data (line graphs).

excitation on a linear scale. In addition to the photoemission peak at 2.25 eV a peak is seen at 2.95 eV final-state energy. Assuming the same excitation pathway as for the peak at 2.25 eV, i.e., single-photon photoemission from the state, this corresponds to a state with a binding energy of 0.15 eV. The presence of two unoccupied states with 0.85 ± 0.05 eV and 0.15 ± 0.05 eV binding energy leads to their identification as the $n=1$ and $n=2$ image potential states.

The binding energies $E_b(n)$ of the hydrogenic bound image potential states are described by the following equation,[15] where n is the quantum number and a is the quantum defect

$$E_b(n)=\frac{0.85\ \text{eV}}{(n+a)^2},\quad n=1,2,\ldots. \tag{1}$$

From the energy difference of 0.7 eV between the $n=1$ and $n=2$ image potential state a quantum defect of $a=-0.04\pm0.05$ is obtained. This demonstrates that the image potential states on graphite exhibit an almost ideal hydrogenlike behavior. A more detailed discussion is presented in Sec. IV.

C. Lifetime of the $n=1$ image potential state

1. Time-resolved two-color photoemission spectroscopy

On the basis of the known excitation pathways in multiphoton photoemission on HOPG with 267 and 400 nm light the results of two-color pump-probe experiments can now be analyzed. In a two-color time-resolved 2P-PES experiment the $n=1$ image potential state can be populated by a 267 nm pump-photon, and the subsequent photoemission by the 400 nm probe-photon leads to the photoemission of an electron with 2.25 eV final-state energy. A pump-probe spectrum for a final-state energy of 2.25 eV is shown in Fig. 7 together with spectra for 0.25 eV lower and 0.35 eV higher final-state energy. The latter two spectra are symmetric with respect to zero delay time. In contrast, the finite lifetime of the image potential state leads to a shift and a slightly asymmetric broadening of the pump-probe signal. The maximum is shifted by 40 fs relative to zero delay time towards positive

delay. This confirms that the 267 nm pulse acts as the pump pulse. Both observations, the shift and the small asymmetry, indicate that the intermediate state has a significant lifetime in the order of the pulse duration. A similar shift of the pump-probe spectrum in time-resolved two-color 2P-PES of image potential states has been reported by Schoenlein *et al.*,[1] Hertel *et al.*,[2] and Shumay *et al.*[5]

The two-color pump-probe signal is composed of several contributions: One originating from the 267 nm-pump and 400 nm-probe process and a second one originating from the reversed absorption sequence. In addition to the resonant excitation via the $n=1$ image potential state, bulk states at the same energy might also contribute to the pump-probe signal. *A priori* it is not possible to distinguish between these contributions. However, to allow an unambiguous determination of the lifetimes of intermediate states it is necessary to separate them. By fitting each spectrum with a Lorentzian peak shape and an exponentially decreasing background (compare Fig. 6) we can determine the background contribution and the area of the resonant photoemission peak for every pump-probe delay separately. The latter contribution as a function of the pump-probe delay reflects exclusively the dynamics of the $n=1$ image potential state, whereas the background gives information on the dynamic behavior of the involved bulk states. The comparison of the pump-probe signals for the $n=1$ image potential state with that of the total photoemission yield at 2.25 eV shows that the photoemission via the 400 nm-pump and 267 nm-probe sequence or via bulk states with 0.85 eV binding energy, has in this case no significant influence.

Since a finite lifetime of an intermediate state leads to a shift of the maximum of the two-color pump-probe signal, it is crucial to unambiguously identify absolute zero delay. On the Cu(111) surface it has been demonstrated that the nonresonant two-photon excitation from the occupied surface state can be used.[2] On graphite the situation is slightly more complicated. The pump-probe signals at final-state energies for which the intermediate states have a lifetime short enough so that they represent the pure cross correlation width of pump and probe pulses can be used as a reference for the absolute zero delay. The pump-probe signals at 2.0 and 2.6 eV final-state energy represent our best choice for this. In the following it will be shown that lifetime effects play only a negligible effect for these pump-probe signals.

The pump-probe signals at zero delay include both possible excitation sequences, 267 nm pump−400 nm probe and 400 nm pump−267 nm probe. Therefore, a pair of intermediate states separated by 1.55 eV is involved. One can expect from Fermi-liquid theory[37] that the intermediate state with the lowest energy, i.e., 1.85 eV, should exhibit the longest lifetime. A relaxation lifetime of about 20 fs at 1.85 eV above the Fermi energy is known from literature.[6,31] Since there is almost no difference between the pump-probe signals at 2.0 and 2.6 eV final-state energy we conclude that there is only negligible lifetime broadening and a shift of the pump-probe spectra due to this fast relaxation of the lower-lying intermediate states. This is additionally supported by the two-color pump-probe signal recorded on a polycrystalline tantalum surface for intermediate states 2 eV above the Fermi energy (shaded area in Fig. 8). For these states the relaxation lifetime is known to be less than 10 fs,[38] and significant lifetime broadening and shift of the pump-probe signal can be excluded.

Besides the shift and the broadening of the pump-probe signal at 2.25 eV it is worth noting an additional detail. Whereas the signal is zero at large negative delay a contribution of about 5% remains at positive delay of more than 200 fs and decays on a ps time scale. This small contribution is attributed to the electron dynamics in states at about 0.55 eV above the Fermi energy that are populated by the 267 nm pump pulse and then photoemitted by a two-photon probe process. On time scales in the order of ps the relaxation behavior in states close to the Fermi energy is dominated by the cooling of the electron gas due to the electron-phonon interaction. This gives rise to the small longlived contribution to the pump-probe signal.

2. Optical Bloch equations

Since the lifetime of the $n=1$ image potential state is in the order of the pulse duration its effect on the pump-probe effect is primarily seen in a shift of the pump-probe signal at 2.25 eV final-state energy with respect to the pure cross correlation of the 267 and 400 nm laser pulses. It has recently been shown that the shift of the pump-probe signal in a time-resolved two-color photoemission experiment can be used to accurately determine the lifetime of the involved state.[2,5] Since pump and probe pulse overlap it is not possible to describe the multiphoton photoemission response of the system by a rate equation model, but the coherent character of the excitation must be considered and therefore the use of the optical Bloch equations for a multilevel system is required.[39] Under the assumption that the coherence in the final state is immediately lost, it is sufficient to use the Bloch equations for a two-level system, as it was shown by Hertel *et al.*[2]

The optical Bloch equations for a two-level system are derived from the equation of motion for the density matrix in the energy representation. The relaxation towards the thermal equilibrium is treated in the phenomenological relaxation time approximation, that assumes time-independent relaxation rates. The population decay of the excited state is described by T_1 and the decay of the polarization by the transversal relaxation time T_2. In the absence of phase-destroying elastic-scattering events but a finite lifetime T_1 of the excited state, the transversal relaxation time T_2 reflects the dephasing of the polarization due to the different spectral components of a lifetime broadened state. Under excitation conditions where population transfer back to the ground state is not yet significant it can be shown that the relation $T_2=2T_1$ must hold.[39] In the presence of phase-destroying scattering events with a dephasing time T_φ, however, the reduced transversal relaxation time T_2 is given by[39]

$$T_2=\left(\frac{1}{2T_1}+\frac{1}{T_\varphi}\right)^{-1}. \tag{2}$$

In the slowly varying envelope approximation which leads to the rotating-wave approximation and with the dipole approximation for the optical excitation of the two-level system, one obtains a set of coupled differential equations[2] that are solved by numerical integration. Since the initial state in the present case is in the continuum of occupied states of graphite, we assume resonant excitation of the excited state.

To obtain the photoemission signal as a function of pump-probe delay the population in the excited state is convoluted with a Gaussian pulse shape that corresponds to the probe pulse duration.

It is important to carefully determine the input parameters for the optical Bloch equations in order to obtain reliable results for the intermediate state lifetime. As discussed in Sec. III C 1, the position of absolute zero delay and the cross correlation width for pump and probe pulses can be determined from the pump-probe signal at a somewhat lower and higher final-state energy (compare Fig. 7). The calculation of the pump-probe signal, however, requires the knowledge of the duration of both pulses. Since we have no direct measure for the duration of the 400 nm pump pulse it is impossible to determine the probe pulse duration from the measured signal. We have, therefore, simulated the pump-probe signal for several pairs of pump and probe-pulse durations that all result in the same cross correlation width. For an intermediate lifetime of about 40 fs this shows that the shape of the pump-probe signal is only slightly changed as long as the pump and probe pulse durations are changed by less than 50%. In order to keep the number of free parameters small we have, therefore, assumed identical pulse durations for pump and probe pulse. The best fit of the pump-probe signal at 2.0 and 2.6 eV final-state energy is shown in Fig. 7 as dotted lines underneath the open symbols and reveals a pulse duration of 90 fs.

The observed linewidth of a photoemission peak is due to homogeneous and inhomogeneous broadening and due to the finite energy resolution of the spectrometer. In the description of the two-photon photoemission process with Bloch equations an inhomogeneous linewidth cannot be distinguished from a system with a T_2 time decreased due to elastic scattering events. In a 2P-PES experiment the linewidth corrected for spectral resolution must therefore directly correspond to the transversal relaxation time T_2. Since the 60 meV energy resolution of the spectrometer increases the linewidth Γ of the photoemission peak (Fig. 6) only by 20 meV we can estimate the value of T_2 from the deconvoluted photoemission linewidth of 170 meV using the relation $T_2 = \hbar/\Gamma$ and obtain $T_2 = 8 \pm 2$ fs. The error represents the variation of Γ in different measurements.

The only free input parameter left is the lifetime T_1 of the intermediate state. Under the assumption of $T_2 = 8$ fs and a pulse duration of 90 fs for pump and probe pulse we obtain the best fit of the pump-probe signal with a lifetime T_1 of the $n=1$ image potential state of 40 fs. From the variation of the mean square error between the theoretical curve and the experimental data as a function of T_1 one can estimate the 68.6% confidence interval as $34\,\text{fs} < T_1 < 46\,\text{fs}$. The best fit varying T_1 and T_2 is achieved with $T_1 = 40$ fs and $T_2 = 10$ fs with their 68.6% confidence intervals given by $28\,\text{fs} < T_1 < 46\,\text{fs}$ and $8\,\text{fs} < T_2 < 45\,\text{fs}$. Obviously it is impossible to obtain an estimate for T_2 from the variation of both parameters since they are strongly correlated. However, the best fit of T_2 agrees with the value determined from the linewidth of the photoemission peak.

IV. DISCUSSION AND CONCLUSION

Summarizing the experimental results, we have unambiguously identified the $n=1$ and $n=2$ image potential state on graphite. Their binding energies are 0.85 and 0.15 eV, respectively. Time-resolved two-color 2P-PES reveals a lifetime of 40 ± 6 fs for the $n=1$ state. In addition we find that the multiphoton photoemission spectra obtained after 400 and 267 nm excitation are consistent with the known bulk band structure of graphite.[17] An energy diagram that schematically represents the projected band structure and the most relevant multiphoton excitation processes is shown in Fig. 8. It is obvious that the two-photon photoemission process via the $n=1$ image potential state must include a non-$k_\parallel$-conserving transition.

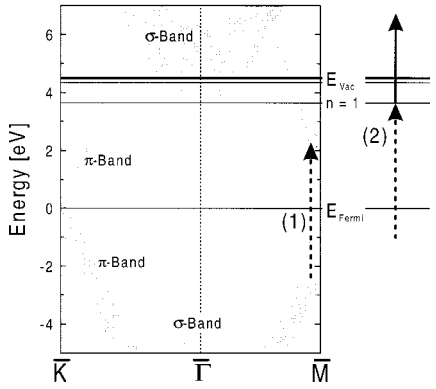

FIG. 8. Projected band structure of graphite derived from Ref. 17 under the assumption that the band dispersion perpendicular to the surface exhibits a monotonous behavior. The occupied σ band is shifted downwards by 1 eV to achieve agreement with experimental results (Ref. 35). The energetic position of the vacuum energy and the $n=1$ and $n=2$ image potential state are indicated by vertical lines. The critical transition with 267 nm light at the M and L point in the band structure (1) and the two-photon excitation via the $n=1$ image potential state with 267 nm-pump and 400 nm-probe process (2) is represented schematically by arrows.

The interaction between the image potential states and the unoccupied bulk band structure determines the binding energy of the states and their electronic relaxation behavior. Their properties therefore give information about the unoccupied bulk band structure and vice versa. As shown in Sec. III B the image potential states on graphite are characterized by a vanishing quantum defect a. The multiple-reflection approach for image potential states[40] allows to relate a to the electronic properties of the substrate. A quantum defect of $a=0$ corresponds to wave functions of the image potential states which have a node at the termination plane that is located half a lattice constant above the surface atoms and a pronounced s-like tail into the bulk. One-dimensional wave function calculations[15] and the multiple reflection approach[40] show that such wave functions are only found if real s-like solutions for the bulk states exist at energies close to the binding energy of the image potential state. The quantum defect a is therefore a measure for the energy difference between the image potential state and bulk states in the projected bulk band structure. This theoretical description neglecting the explicit structure of the surface is in agreement with the observations for quite a number of metal surfaces.[13,15] According to this, the vanishing quantum defect for the image potential states on graphite leads to the conclusion that the $n=1$ state seen at 3.65 eV above the Fermi energy is energetically close to a s-like bulk band. Since

there is no evidence for *s*-like bands at energies below 3.7 eV,[17] we derive from the vanishing quantum defect that the lowest unoccupied σ band is located at about 3.7 eV above the Fermi energy. This is in agreement with those bulk band-structure calculations that predict the minimum of the interlayer band at this energy.[17,24]

The existence of the $n=1$ image potential state and its small difference in energy with respect to the minimum of the interlayer band answers the question about the origin of the feature seen in inverse photoemission at about 3.7 eV above the Fermi energy.[18,19,22] Due to the limited energy resolution in these experiments and since non-$k_{\parallel}$-conserving transitions cannot be excluded it has been impossible to distinguish between bulk and surface contributions, i.e., the signal from the interlayer band and the $n=1$ image potential state. The observation that the feature at about 3.7 eV is sometimes influenced by surface modification[22] and sometimes not[19] can be explained by different sensitivity to either the surface state or the bulk band contribution in different experiments.

The vanishing quantum defect of the image potential state for graphite sheds light on the nature of surface states of layered materials in general. In addition to non-$k_{\parallel}$-conserving transitions Fauster *et al.* has proposed a surface state split-off from the interlayer band to explain the ARIPES results.[18] Calculations using an effective potential derived from an *ab initio* treatment of a single carbon plane that includes electron correlation effects predict such a state just below the minimum of the interlayer band.[41] This illuminates that on graphite the $n=1$ image potential state could be viewed also as a splitoff state from the unoccupied σ band. This correspondence is due to the fact that the unoccupied band structure in graphite exhibits a two-dimensional character and that the interaction of an excited bulk electron with all other electrons in the layer determines its energy in a similar way as it is the case for an image potential state. This close relation between image potential states and the unoccupied *s*-like bands could, therefore, help to improve the understanding of collective phenomena in graphite or in layered materials in general.

The image potential state lifetime is determined by the interaction with bulk states and by the carrier relaxation in the substrate. A long lifetime reflects a small overlap with the bulk states or a long lifetime of the bulk states. In order to decide what determines the image potential state lifetime of 40 fs on graphite it is necessary to compare it with other known lifetimes. A lifetime of 40 and 55 fs has been determined recently for the $n=1$ image potential state on Cu(100) and Ag(100), respectively.[5] In both cases, however, the image potential state is located at about midgap in the projected band structure. Therefore, these states have small overlap with bulk states, resulting in a rather long lifetime. In contrast, the image potential state on graphite is located close to the minimum of the unoccupied σ band and should be compared for example with the $n=1$ image potential state on Cu(111) having a lifetime of about 15 fs.[2,5] Taking this into account, the lifetime on graphite is much longer than those found on metal surfaces. This could either indicate a weak interaction between the image potential state and the bulk bands although the state is located at the top of the band gap or a long relaxation lifetime of the electrons in the corresponding bulk band. The latter explanation is related to the two-dimensional character of the bulk band structure in graphite, since the localization of the interlayer band wave functions between the carbon planes reduces the overlap with final states of the relaxation process. However, a clear identification of the physical mechanism requires a theoretical treatment of the image potential states on graphite that includes band-structure effects. The feasibility of this has been demonstrated recently for the Cu(100) and Cu(111) surfaces.[42]

In conclusion, multiphoton photoemission on graphite at 400 and 267 nm excitation allowed the unambiguous identification of the $n=1$ and $n=2$ image potential state on graphite. The observed binding energies of 0.85 and 0.15 eV, respectively, and the corresponding quantum defect of $a=0$ show that the $n=1$ image potential state is located close to the top of the band gap of the projected band structure. This observation settles the controversy concerned with the unoccupied band structure of graphite. Both the minimum of the interlayer band and the $n=1$ image potential state give rise to a feature seen in inverse photoemission at about 3.7 eV above the Fermi energy and cannot be resolved in those experiments. Time-resolved 2P-PES reveals a lifetime of 40 ± 6 fs for the $n=1$ image potential state. We relate the location of the $n=1$ image potential state close to the top of the band gap and its rather long lifetime to the two-dimensional character of the interlayer band. Additional experiments on other layered materials and theoretical investigations of the surface states in quasi-two-dimensional systems should lead to an improved understanding of the dynamic properties of a layered electron gas.

*FAX: 0931-888-4906. Electronic address: pfeiffer@physik.uni-wuerzburg.de

[1] R. W. Schoenlein, J. G. Fujimoto, G. L. Eesley, and T. W. Capehart, Phys. Rev. Lett. **61**, 2596 (1988).
[2] T. Hertel, E. Knoesel, M. Wolf, and G. Ertl, Phys. Rev. Lett. **76**, 535 (1996).
[3] U. Höfer, I. L. Shumay, C. Reuss, U. Thomann, W. Wallauer, and Th. Fauster, Science **277**, 1480 (1997).
[4] R. M. Osgood, Jr. and Xiaoyi Wang, in *Solid State Physics: Advances in Research and Applications*, edited by H. Ehrenreich and F. Spaepen (Academic, New York, 1998), Vol. 51, p. 1.
[5] I. L. Shumay, U. Höfer, Ch. Reuss, U. Thomann, W. Wallauer, and Th. Fauster, Phys. Rev. B **58**, 13 974 (1998).
[6] K. Ertel, U. Kohl, J. Lehmann, M. Merschdorf, W. Pfeiffer, A. Thon, S. Voll, and G. Gerber, Appl. Phys. B: Lasers Opt. **68**, 439 (1999).
[7] W. Schockley, Phys. Rev. **56**, 317 (1939).
[8] P. M. Echenique and J. B. Pendry, J. Phys. C **11**, 2065 (1978).
[9] E. G. McRae, Rev. Mod. Phys. **51**, 541 (1979).
[10] P. D. Johnson and N. V. Smith, Phys. Rev. B **27**, 2527 (1983).
[11] V. Dose, W. Altmann, A. Goldmann, U. Kolac, and J. Rogozik, Phys. Rev. Lett. **52**, 1919 (1984).
[12] D. Straub and F. J. Himpsel, Phys. Rev. Lett. **52**, 1922 (1984).
[13] D. Straub and F. J. Himpsel, Phys. Rev. B **33**, 2256 (1986).
[14] W. Steinmann, Appl. Phys. A: Solids Surf. **49**, 365 (1989).
[15] W. Steinmann and Th. Fauster, Adv. Ser. Phys. Chem. **5**, 184

(1995).
[16] R. W. Schoenlein, J. G. Fujimoto, G. L. Eesley, and T. W. Capehart, Phys. Rev. B **43**, 4688 (1991).
[17] J. C. Boettger, Phys. Rev. B **55**, 11 202 (1997).
[18] Th. Fauster, F. J. Himpsel, J. E. Fischer, and E. W. Plummer, Phys. Rev. Lett. **51**, 430 (1983).
[19] B. Reihl, J. K. Gimzewski, J. M. Nicholls, and E. Tossati, Phys. Rev. B **33**, 5770 (1986).
[20] T. Takahashi, H. Tokailin, and T. Sagawa, Phys. Rev. B **32**, 8317 (1985).
[21] F. Maeda, T. Takahashi, H. Ohsawa, and S. Suzuki, Phys. Rev. B **37**, 4482 (1988).
[22] I. Schäfer, M. Schlüter, and M. Skibowski, Phys. Rev. B **35**, 7663 (1987).
[23] R. Claessen, H. Cartensen, and M. Skibowski, Phys. Rev. B **38**, 12 582 (1988).
[24] N. A. W. Holzwarth, S. G. Louie, and S. Rabii, Phys. Rev. B **26**, 5382 (1982).
[25] R. C. Tatar and S. Rabii, Phys. Rev. B **25**, 4126 (1982).
[26] I. R. Collins, P. T. Andrews, and A. R. Law, Phys. Rev. B **38**, 13 348 (1988).
[27] R. Yen, J. M. Liu, N. Bloembergen, T. K. Yee, J. G. Fujimoto, and M. M. Salour, Appl. Phys. Lett. **40**, 185 (1982).
[28] R. T. Williams, R. R. Royt, J. C. Rife, J. P. Long, and M. N. Kabler, J. Vac. Sci. Technol. **21**, 509 (1982).
[29] H. Petek and S. Ogawa, Prog. Surf. Sci. **56**, 239 (1997).
[30] H. Petek, A. P. Heberle, W. Nessler, H. Nagano, S. Kubota, S. Matsunami, N. Moriya, and S. Ogawa, Phys. Rev. Lett. **79**, 4649 (1997).
[31] S. Xu, J. Cao, C. C. Miller, D. A. Mantell, R. J. D. Miller, and Y. Gao, Phys. Rev. Lett. **76**, 483 (1996).
[32] MATECK, Material-Technologie & Kristalle GmbH, Jülich, Germany. The used HOPG is characterized by a mosaic spread of smaller than 1.5.
[33] SIMION 3D, Version 6.0, Princeton Electronic Systems, 1995.
[34] R. Klucker, M. Skibowski, and W. Steinmann, Phys. Status Solidi B **65**, 703 (1974).
[35] W. Eberhardt, I. T. McGovern, E. W. Plummer, and J. E. Fisher, Phys. Rev. Lett. **44**, 200 (1980).
[36] A. R. Law, M. T. Johnson, and H. P. Hughes, Phys. Rev. B **34**, 4289 (1986).
[37] D. Pines and P. Nozieres, *The Theory of Quantum Liquids* (Benjamin, New York, 1966).
[38] M. Aeschlimann, S. Pawlik, and M. Bauer, Ber. Bunsenges. Phys. Chem. **99**, 1504 (1995).
[39] M. D. Levenson and S. S. Kano, *Nonlinear Laser Spectroscopy* (Academic, San Diego, 1988).
[40] N. V. Smith, Phys. Rev. B **32**, 3549 (1985).
[41] M. Posternak, A. Baldereschi, A. J. Fremann, and E. Wimmer, Phys. Rev. Lett. **52**, 863 (1984).
[42] E. V. Chulkov, I. Sarría, V. M. Silkin, J. M. Pitarke, and P. M. Echenique, Phys. Rev. Lett. **80**, 4947 (1998).